	Retinorecipient targets						
RGC subtype	SCN	vLGN	dLGN	OPN	NOT	MTN	SC
M1 ipRGCs	+++	+++		+++ (shell)			+
M2 ipRGCs	+			+++ (core)			
M4 ipRGCs			+++ (core)				+++ (lSGS)
t-Off α RGCs			+++ (core)				+++ (lSGS)
On-Off DSGCs		+	++ (shell)				+++ (uSGS)
Hoxd10-RGCs			+ (shell)		+++	+++	+ (uSGS)

CNTN4 protein expression in retinorecipient targets

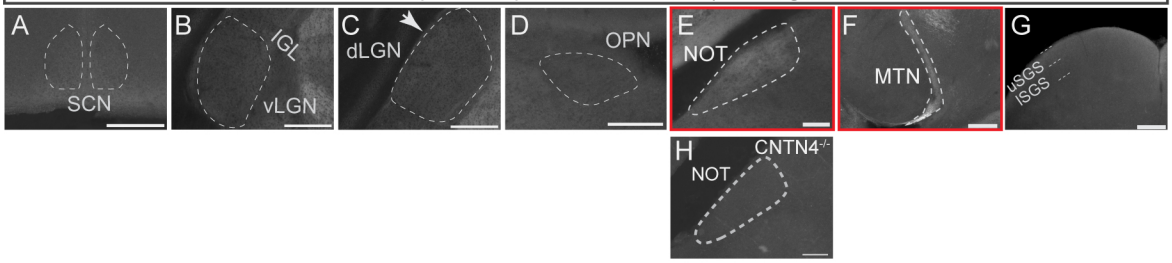

Figure S1: Specificity of CNTN4 expression in RGC subtypes and their visual targets (related to Figure 1).

Chart of the major RGC subtypes (listed on left) and their retinorecipient targets. Targets with dense innervation: +++, moderate innervation: ++, and sparse innervation: +. The absence of any symbol indicates a complete lack of input to that target. References for these patterns: M1 ipRGCs (Hattar et al., 2006), M2 and M4 ipRGCs (Ecker et al., 2010; Estevez et al., 2012; Osterhout et al., 2014), t-Offα RGCs (Huberman et al., 2008; 2009), On-Off DSGCs (Huberman et al., 2009; Rivlin-Etzion et al., 2011), Hoxd10 (slow-tuned AOS projecting On-DSGCs (3 subtypes) and On-Off DSGC (one subtype) (Dhande et al., 2013; and this study).

(A-G) CNTN4 protein expression in the major retinorecipient targets. CNTN4 is either absent or expressed at very low levels in retinorecipient areas other than the NOT and MTN. These targets are only innervated by Hoxd10 On-DSGCs and one subtype of slow tuned On-Off DSGC, all of which are labeled in Hoxd10-GFP mice (and see Dhande et al., 2013 and main Figures, and S3 below.)

(A, B, D) CNTN4 expression is absent from the hypothalamic suprachiasmatic nucleus (SCN, A), and ventral lateral geniculate nucleus (vLGN, B) and intergeniculate leaflet (IGL, B) olivary pretectal nucleus (OPN; D).

(C) CNTN4 is expressed at very low levels in one subregion of the dorsal lateral geniculate nucleus (dLGN), the shell (arrow in (B)). Previous studies indicate this region receives sparse input from Hoxd10-RGCs (Dhande et al., 2013; Osterhout et al., 2014). Scale = 250μm

(E-F) CNTN4 expressed in NOT and MTN; Scale = 250μm

(G) CNTN4 is expressed at low levels in superficial retinorecipient superior colliculus (SC), the upper stratum griseum superficialis (uSGS). This subregion of the SC is known to receive sparse input from Hoxd10-RGCs (Dhande et al., 2013). lSGS: lower stratum griseum superficialis; Scale = 500μm

(H) Antibody expression is specific. CNTN4 is not expressed in the NOT (or elsewhere in the brain or retina) in CNTN4$^{-/-}$ mice (H). Scale = 200μm
Note: these expression patterns are all consistent with the argument that CNTN4 protein is expressed by Hoxd10-RGCs that mainly target the AOS nuclei, but not by other major groups of RGC subtypes that target other retinofugal targets.

Supplemental Figure 2

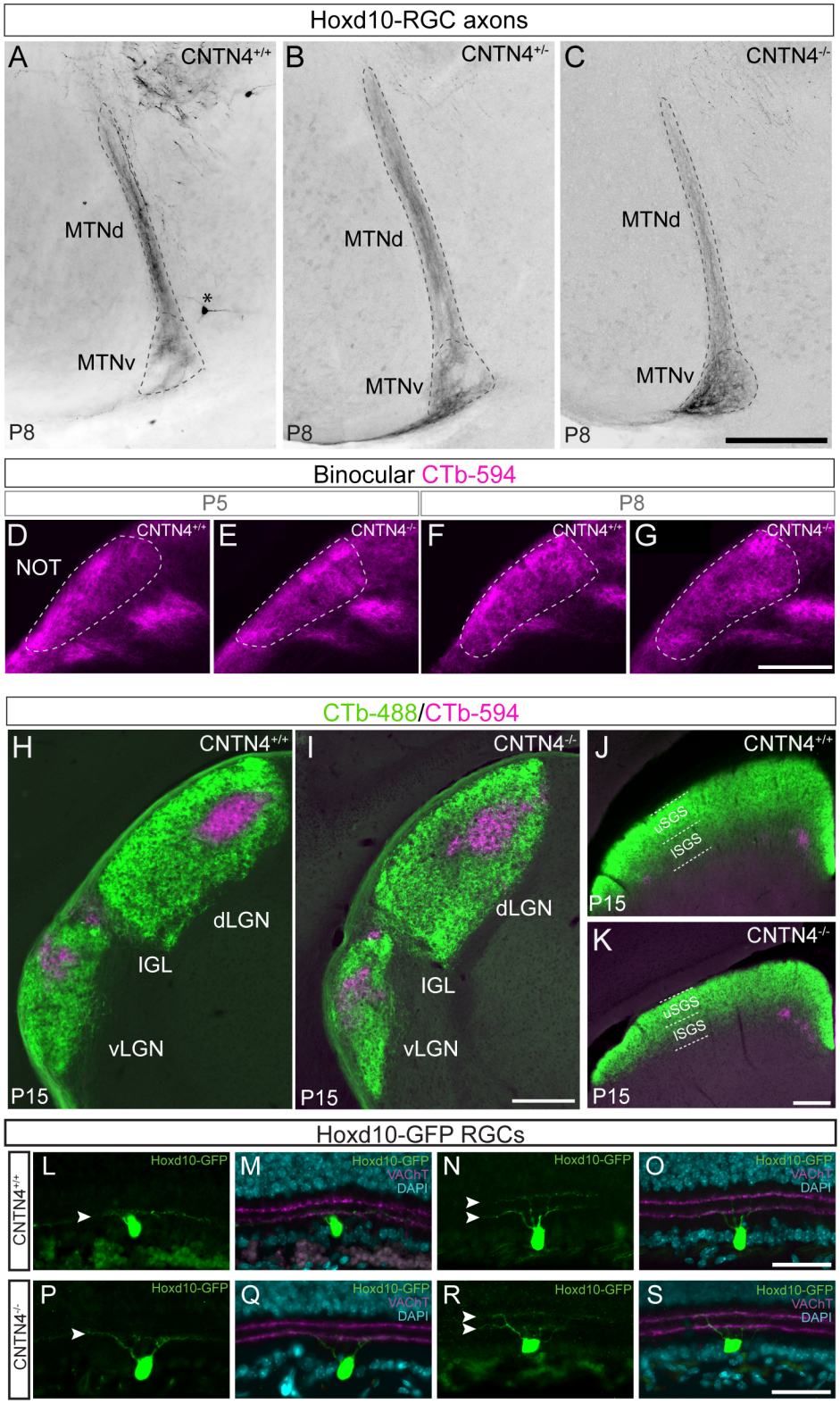

Figure S2: CNTN4$^{-/-}$ Hoxd10-RGCs innervate the MTN and other retinorecipient targets normally, and their dendrites stratify correctly (related to Figure 2).

(A-C) Hoxd10-RGC axons in the MTN of (A) wildtype, (B) CNTN4$^{+/-}$, and (C) CNTN4$^{-/-}$ mice. Age P8 is shown. Scale = 250µm

(D-G) Whole eye binocular labeling with CTb-594 at P5 and P8 reveals similar timing and pattern of overall RGC innervation of the NOT for wildtype (D, F) and CNTN4$^{-/-}$ mice (E, G). P5 and P8 timepoints are shown, which correspond to when this pretectal region receives it major input from retina (see Osterhout et al., 2014 for details). Scale = 250µm

(H-K) CTb-594 (ipsilateral eye) and CTb-488 (contralateral eye) projections to the visual thalamic targets dLGN, IGL and vLGN (H,I) and to the SC (J,K) in wildtype (H, J) and CNTN4 mutant (I, K) mice. In both areas of the retinofugal pathway RGCs (as a general population) innervate retinorecipient targets and refine to the correct laminar zones, irrespective of genotype. All targets are filled completely and binocular segregation appears normal (e.g., ipsilateral eye projections to SC are in area ventral to lSGS.) Scale = 250µm

(L-S) Dendritic stratification of monostratified Hoxd10-GFP On-DSGCs (L,M,P,Q) and bistratified Hoxd10-GFP On-Off DSGCs in (N, O, R, S) wildtype CNTN4$^{+/+}$ (L-O) and mutant CNTN4$^{-/-}$ mice (P-S). Scale = 50µm. For details on these types of RGCs expressing GFP in Hoxd10 mice, see Dhande et al., 2013 and Supplemental Figure 3.

Supplemental Figure 3

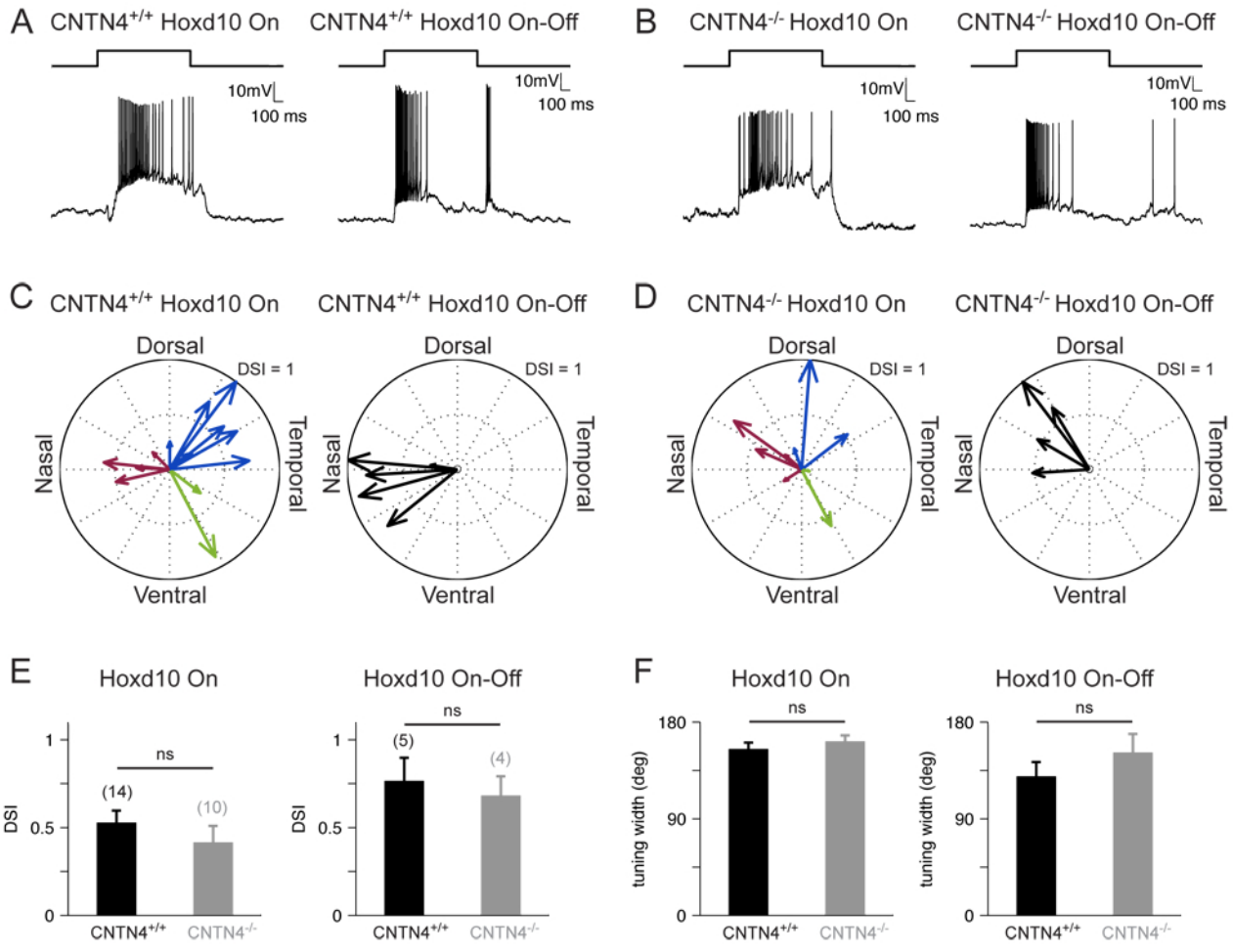

Figure S3: Loss of CNTN4 does not alter functional output or receptive field properties of Hoxd10-GFP RGCs (related to Figure 3).

(A) Whole-cell, current-clamp recordings from a WT On (top, left) and On-Off (top, right) Hoxd10-GFP RGC in response to a 300 μm and 200 μm diameter spot respectively, presented for 1 sec, and centered on the receptive field center. Trace above the voltage trace corresponds to the timing of the light stimulus.

(B) Same as in (A) for Hoxd10-GFP RGCs in a CNTN4$^{-/-}$ background. The responses of the cells are normal.

(C) Summary polar plots for WT On (left) and On-Off (right) Hoxd10-GFP RGCs. Arrows represent responses from individual cells to presentations of square-wave drifting gratings in 12 different directions (see Experimental procedures). The angle of each arrow represents the directional preference of the cell and the length represents the DSI, or the strength of the directional tuning. On Hoxd10-GFP RGCs can be grouped into three types that respond to Nasal (red), Dorsal-Temporal (blue), and Ventral-Temporal (green) motion, while On-Off Hoxd10-RGCs only respond to Nasal motion.

(D) Same as in (C) for Hoxd10-GFP RGCs in a CNTN4$^{-/-}$ background. There is no significant difference in the angle of the directional preference of On and On-Off Hoxd10-GFP RGCs as compared to WT cells ($p > 0.3$ for all; Watson-Williams Test).

(E) Quantification and comparison of the DSI for On and On-Off Hoxd10-GFP RGCs. There is no significant difference between CNTN4$^{-/-}$ and WT RGCs (On: $p = 0.3$; On-Off: $p = 0.7$; t-test). Number of cells analyzed in parentheses. Error bars indicate SEM.

(F) Quantification and comparison of tuning width On and On-Off Hoxd10-GFP RGCs. There is no significant difference between CNTN4$^{-/-}$ and WT RGCS (On: $p = 0.4$; On-Off: $p = 0.3$; t-test). Error bars indicate SEM. Number of cells analyzed in parentheses (same as in E).

Supplemental Figure 4

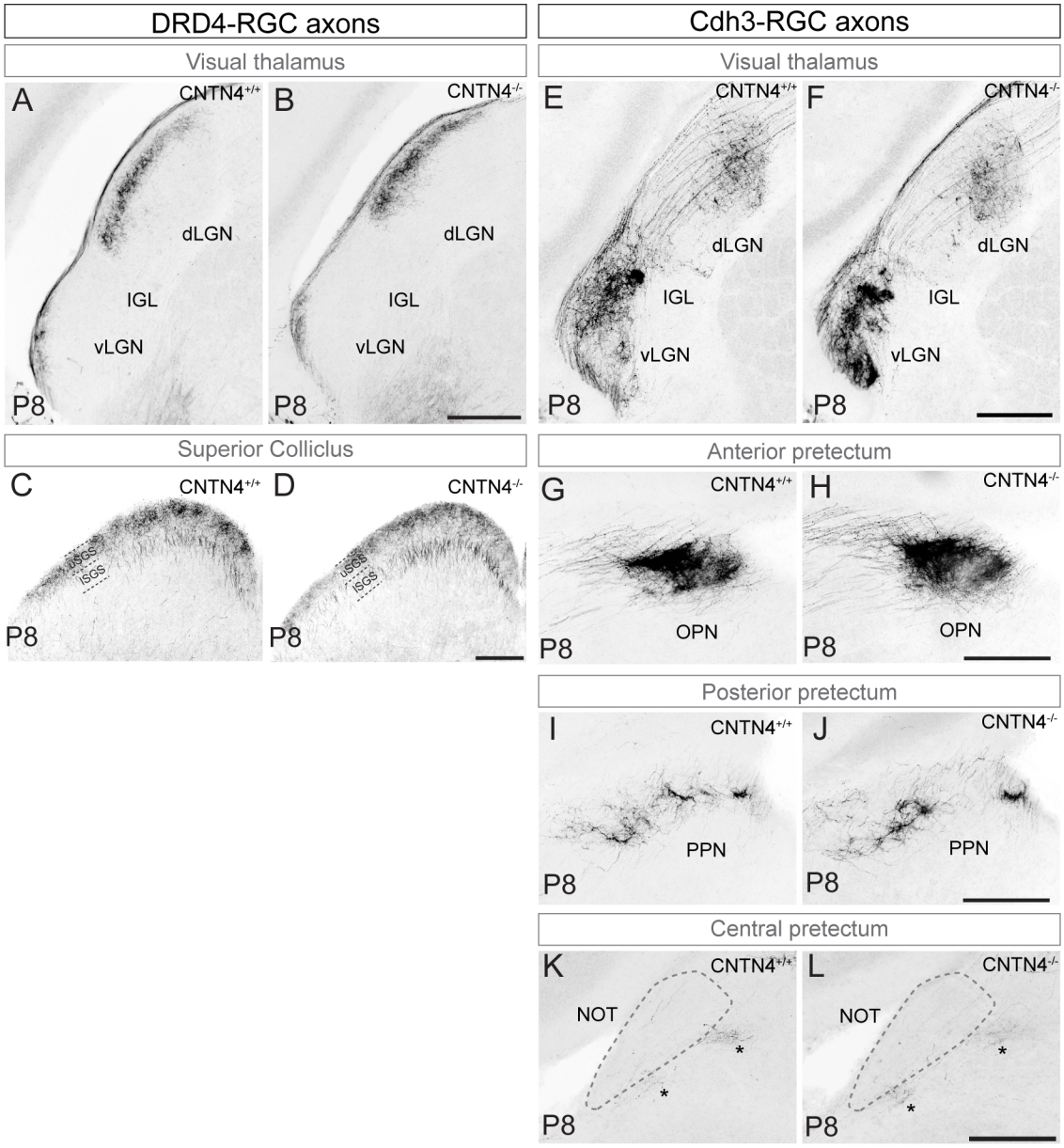

Figure S4: Axon-target matching by non-AOS projecting RGCs appears normal (related to Figure 4).

(A-D) DRD4-GFP RGC axons correctly innervate the shell region of the dLGN (A, B) and the uSGS of the SC (C,D) in both wildtype (A,C) and CNTN4$^{-/-}$ (B, D) mice.

(E-L) Cdh3-GFP RGC axons correctly innervate the visual thalamus (E, F), anterior pretectum OPN (G, H), posterior pretectum PPN (I, J) and central pretectum NOT (K, L) in wildtype (E, G, I, K) and CNTN4$^{-/-}$ (F, H, J, L) mice. All Scale = 250μm.

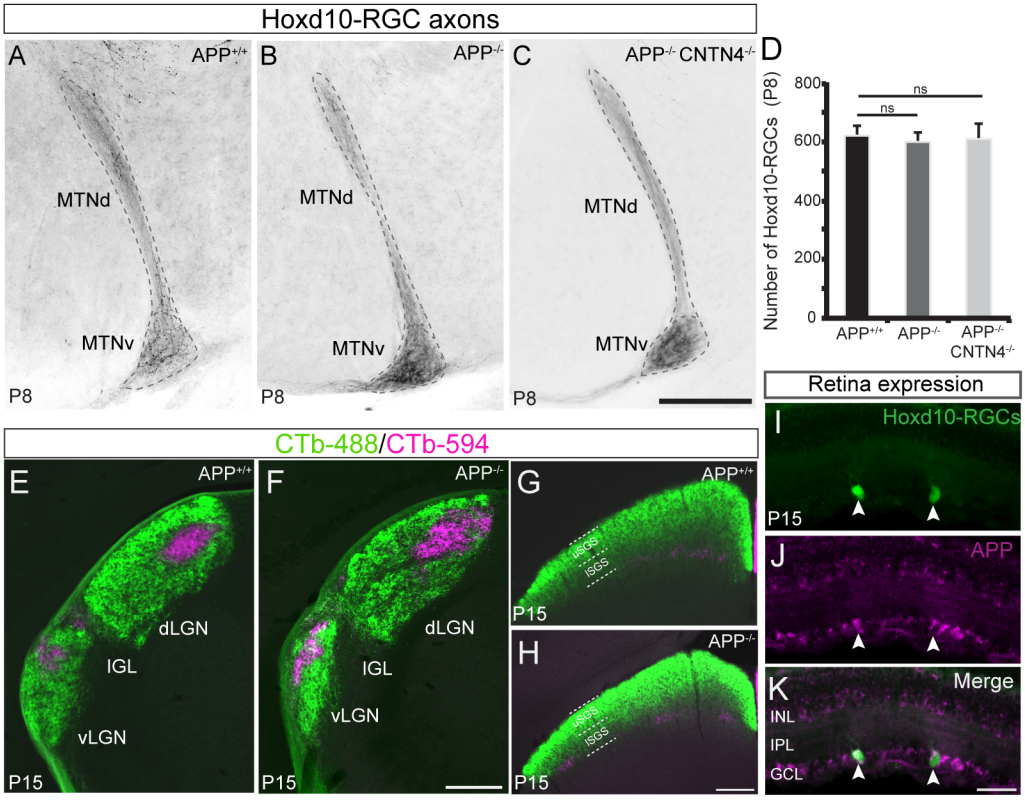
Hoxd10-RGC axons
A
APP+/+
MTNd
MTNv
P8
B
APP-/-
MTNd
MTNv
P8
C
APP-/- CNTN4-/-
MTNd
MTNv
P8
D
Number of Hoxd10-RGCs (P8)
800
600
400
200
0
ns
ns
APP+/+
APP-/-
APP-/- CNTN4-/-
CTb-488/CTb-594
E
APP+/+
dLGN
IGL
vLGN
P15
F
APP-/-
dLGN
IGL
vLGN
P15
G
APP+/+
sSGSp
iSGS
P15
H
APP-/-
sSGSp
iSGS
P15
Retina expression
I
Hoxd10-RGCs
P15
J
APP
K
Merge
INL
IPL
GCL

Figure S5: APP mutant Hoxd10-RGCs innervate the MTN and other retinorecipient targets normally, and Hoxd10-RGC numbers are maintained (related to Figure 6).

(A-C) Hoxd10-RGC axons in the MTN at age P8 in: (A) wildtype $APP^{+/+}$ mice, (B) $APP^{-/-}$ mice, and (C) $APP^{-/-}$ $CNTN4^{-/-}$ double knockout mice (C). Scale = 250µm

(D) Total number of Hoxd10-GFP RGCs in retinas of wildtype $APP^{+/+}$ mice (black bar), $APP^{-/-}$ mice (dark grey), and $CNTN4^{-/-}$, $APP^{-/-}$ double knockout mice (light gray; ±SEM; t-test).(n=5-6 mice per genotype).

(E-H) CTb488/594-labeled RGC axons (as in S2) in the visual thalamus (E, F) and in the SC (G, H) of control (E, G) and (F, H) $APP^{-/-}$ mice. Age P15 shown. Innervation patterns of these targets are normal. Note: the slightly larger ipsilateral sector of the dLGN in APP mutants is within normal range (see Jaubert-Miazza et al., 2005). Scale = 250µm

(I-K) All Hoxd10-RGCs (arrowheads, green signal, I) express APP protein (arrowheads magenta, J). (K) merge of (I and J). The broader expression of APP is expected (see main text). Scale = 100µm.

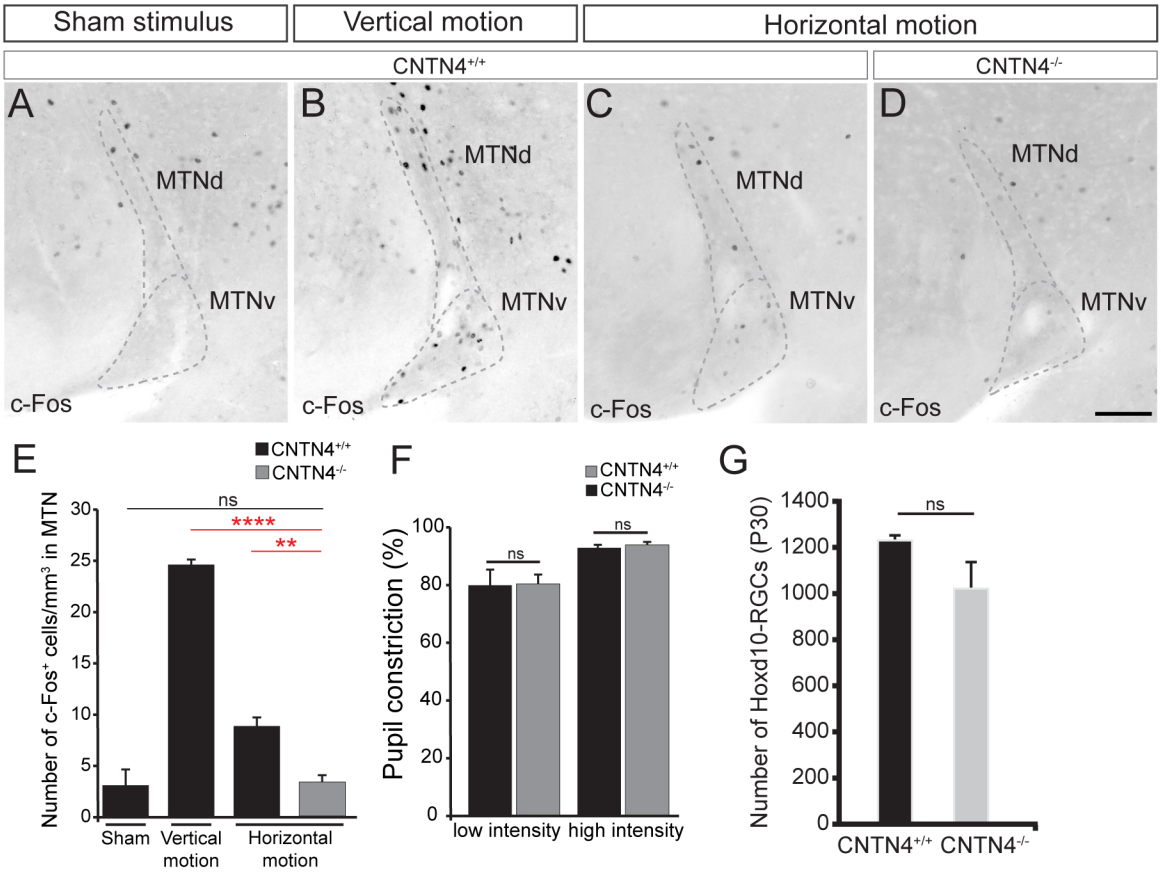
Sham stimulus
Vertical motion
Horizontal motion
CNTN4+/+
CNTN4-/-
A
B
C
D
MTNd
MTNv
c-Fos
E
CNTN4+/+
CNTN4-/-
ns
****
**
Number of c-Fos+ cells/mm3 in MTN
Sham
Vertical motion
Horizontal motion
F
Pupil constriction (%)
low intensity
high intensity
G
Number of Hoxd10-RGCs (P30)
CNTN4+/+
CNTN4-/-

Figure S6: Loss of CNTN4 results in decreased c-Fos activation in the MTN in response to horizontal motion stimuli, but loss of CNTN4 does not alter pupil reflexes (related to Figure 8).

(A-D) c-Fos activation in the MTN of wildtype mice in response to a sham stimulus (A), vertical motion (B), or t horizontal motion (C). (D) c-Fos activation in the MTN of CNTN4$^{-/-}$ mice in response to horizontal motion. Scale = 250μm

(E) Quantification of the number of c-Fos expressing neurons/mm^3 in the MTN of wildtype (black bar) or CNTN4$^{-/-}$ (gray bar) mice in response to sham stimulus or vertical or horizontal drifting gratings. (±SEM; **P<0.01; t-test) (n = 3-5 mice per condition).

(F) Percent reduction in pupil area (a direct measurement of pupil constriction) in response to stimulation with high intensity or low intensity light in wildtype (black bars) and CNTN4$^{-/-}$ (gray bars) mice (n=5 mice per group).
(G) Number of Hoxd10-RGCs in the retina at P30

Supplemental Data References

Dhande, O.S., Estevez, M.E., Quattrochi, L.E., El-Danaf, R.N., Nguyen, P.L., Berson, D.M., and Huberman, A.D. (2013). Genetic dissection of retinal inputs to brainstem nuclei controlling image stabilization. J Neurosci. *33*, 17797–17813.

Dhande, O.S., and Huberman, A.D. (2014). Retinal ganglion cell maps in the brain: implications for visual processing. Curr. Opin. Neurobiol. *24*, 133–142.

Ecker, J.L, Dumitrescu, O.N., Wong, K.Y., Alam, N.M., Chen, S.K., LeGates, T., Renna, J.M., Prusky, G.T., Berson, D.M., Hattar, S. (2010) Melanopsin-expressing retinal ganglion-cell photoreceptors: cellular diversity and role in pattern vision. Neuron *67*, 49-60.

Estevez, M.E., Fogerson, P.M., Ilardi, M.C., Borghuis, B.G., Chan, E., Weng, S., Auferkorte, O.N., Demb, J.B., Berson, D.M. (2012). Form and function of the M4 cell, an intrinsically photosensitive retinal ganglion cell type contributing to geniculocortical vision. J Neurosci. *32*, 13608-20.

Hattar, S., Kumar, M., Park, A., Tong, P., Tung, J., Yau, K.W., Berson, D.M. (2006). Central projections of melanopsin-expressing retinal ganglion cells in the mouse. J Comp Neurol. *497*, 326-49

Huberman AD, Manu M, Koch SM, Susman MW, Lutz AB, Ullian EM, Baccus SA, Barres BA. (2008). Architecture and activity-mediated refinement of axonal projections from a mosaic of genetically identified retinal ganglion cells. Neuron *59*, 425-38.

Huberman, A.D., Wei, W., Elstrott, J., Stafford, B.K., Feller, M.B., and Barres, B.A. (2009). Genetic identification of an On-Off direction-selective retinal ganglion cell subtype reveals a layer-specific subcortical map of posterior motion. Neuron *62*, 327–334.

Jaubert-Miazza, L., Green, E., Lo, F.S., Bui, K., Mills, J., Guido, W. (2005). Structural and functional composition of the developing retinogeniculate pathway in the mouse. Vis Neurosci *22*, 661-76.

Osterhout, J.A., El-Danaf R.N., Nguyen P.L., Huberman A.D. (2014). Birthdate and outgrowth timing predict cellular mechanisms of axon target matching in the developing visual pathway. Cell Reports *8*, 1006-1017.

Rivlin-Etzion, M., Zhou, K., Wei, W., Elstrott, J., Nguyen, P.L., Barres, B.A., Huberman, A.D., Feller, M.B. (2011). Transgenic mice reveal unexpected diversity of on-off direction-selective retinal ganglion cell subtypes and brain structures involved in motion processing. J Neurosci. *31*, 8760–8769.